**SEARCHING FOR WATER ICE AT THE LUNAR NORTH POLE USING HIGH-RESOLUTION IMAGES AND RADAR.** J. L. Mitchell[1], S. J. Lawrence[2], M. S. Robinson[1], E. J. Speyerer[1], and B. W. Denevi[3], [1]School of Earth and Space Exploration, Arizona State University, Tempe, AZ. (Julie.L.Mitchell@asu.edu), [2]NASA Johnson Space Center, Houston, TX, [3]Johns Hopkins University Applied Physics Laboratory, Laurel, MD.

**Introduction:** Permanently shadowed regions (PSRs) at the lunar poles are potential reservoirs of frozen volatiles, and are therefore high-priority exploration targets [**1-4** and others]. PSRs trap water and other volatiles because their annual maximum temperatures (40-100K, [**1**]) are lower than the sublimation temperatures of these species (i.e. $H_2O$ ~104K) [**1**]. Previous studies using various remote sensing techniques have not been able to definitively characterize the distribution or abundance of ice in lunar PSRs. The purpose of this study is to search for signs of ice in PSRs using two complimentary remote sensing techniques: radar and visible images.

**Background:** Numerous PSRs were found to have circular polarization ratios (CPR) considered anomalous because the CPR interior to the crater is high relative to the exterior; these CPR signatures could be the result of significant ice deposits in the crater [**5**]. However, the anomalous CPR signatures could also be the result of wavelength-scale blocks within the crater but not its ejecta. Here we assess the presence or absence of blocks associated with these radar-anomalous craters as an alternative to the ice hypothesis. The Lunar Reconnaissance Orbiter (LRO) Mini-RF instrument actively transmitted circularly-polarized S-band (12.6-cm) radar waves [**6**]. The Lunar Reconnaissance Orbiter Camera (LROC) Narrow Angle Camera (NAC) has obtained long-exposure images of PSR interiors at the 10+ m pixel scale [**7, 8**]. NAC images reveal PSR interiors, allowing the identification of blocks (>20 m diameter) to assess whether the radar signatures are likely due to a rocky crater interior rather than ice.

**Methods:** Water ice deposits and wavelength-scale blocks result in double-bounce backscatter of S-band radar waves. The *m-chi* decomposition [**9**] is used to produce a qualitative distribution of double-bounce backscatter detected by Mini-RF. The *m-chi* decomposition separates radar returns into single-bounce backscatter indicative of features smooth at the wavelength scale, volume scattering such as from randomly-oriented rocks suspended in lunar regolith, and double-bounce backscatter. Often *m-chi* decomposition components are displayed as a colorized map, where single-bounce backscatter is green, volume scattering blue, and double-bounce backscatter red [**9**] (**Fig. 1**).

Radar alone cannot distinguish between young, fresh craters and older craters that contain water ice because both result in high double-bounce backscatter in their interiors. LROC long-exposure NAC images were used to allow a quantitative comparison of blocks between regions with potentially high concentrations of ice and regions definitively without ice. Long-exposure images of PSRs have larger pixel scales than nominal-exposure products (10-20 m/px versus 0.5-1.0 m/px nominal); therefore, only blocks larger than 20-40 m in diameter can be detected. *M-chi* maps and block counts were produced for four CPR-anomalous craters and two CPR-normal craters at the north pole, and two CPR-anomalous equatorial craters (**Table 1**).

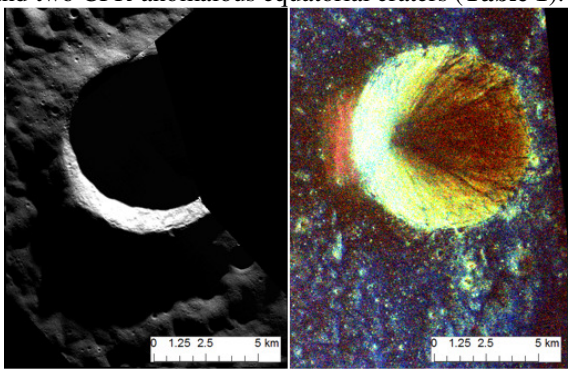


**Fig. 1.** LROC NAC (left) and *m-chi* map (right) of polar CPR-anomalous crater Rozhdestvenskiy N.

**Table 1.** Craters of study. *Whipple was previously reported as pre-Nectarian, but further analysis revealed it to be Imbrian.

| Crater | Lat (°N) | Long (°E) | CPR | Age |
|---|---|---|---|---|
| Rozhdestvenskiy N | 84.04 | 203.73 | Anom. | Copernican |
| Lovelace E | 82.04 | 263.22 | Anom. | Imbrian |
| Lovelace | 82.08 | 250.49 | Anom. | Imbrian |
| Whipple* | 89.14 | 120.05 | Anom. | Imbrian* |
| Main L | 81.44 | 22.73 | Normal | Copernican |
| Plaskett U | 82.41 | 162.29 | Normal | Eratosthenian |
| Byrgius C | 21.17 | 295.49 | Anom. | Copernican |
| Gardner | 17.73 | 33.80 | Anom. | Imbrian |

The standard LROC processing pipeline [**7**] and CraterTools [**10**] were used to characterize block size-frequency distributions (SFDs) at craters with blocks. The SFDs of small (<20 m) blocks in PSR-bearing craters were extrapolated using a power law [**11**]. SFDs allowed a comparison to be made between the numbers of small blocks in PSRs, outside of PSR-bearing craters, and at fully lit equatorial craters. The slope of the log-log plot of the SFD, known as *B* from [**11**], allows a comparison of geologic/erosional processes between sites that have the same composition. Polar CPR-anomalous craters could have *B* values distinct from equatorial CPR-anomalous craters, which cannot have ice due to high daytime temperatures.

**Results:** Rozhdestvenskiy N showed double-bounce backscatter in its interior and no detectable blocks (≥20 m diameter). Other craters where the pres-

ence of ice was proposed [**3, Table 1**] were dominated by single-bounce scattering with patches of double-bounce backscatter and contained <0.2 total detectable blocks per km$^2$. The low quantity of blocks is likely the result of resolution limitations since the majority of visible blocks in equatorial crater interiors were <15 m in diameter. Some craters showed an admixture of block sizes which produced equal parts double-bounce, single-bounce, and volume scattering; this combination of scattering results in a white color in *m-chi* maps.

Of the eight craters included in this study, four had enough blocks in their interiors/PSRs and exteriors/ejecta to allow meaningful extrapolation of SFDs. (**Fig. 2**). For all craters, the quantity of blocks was lower in the crater interior/PSR than the exterior. This trend is possibly an intrinsic property of lunar craters because it persists in both equatorial craters, which do not have ice, and in polar craters. Estimates of the number of small blocks in PSRs, produced by extrapolating a power law (**Fig. 3**), showed no significant variation between equatorial and polar block abundances with the exception of Whipple crater. In addition, there were no significant variations in *B* values between craters, showing that erosional processes likely do not vary significantly between craters with varying radar backscatter properties in these few cases.

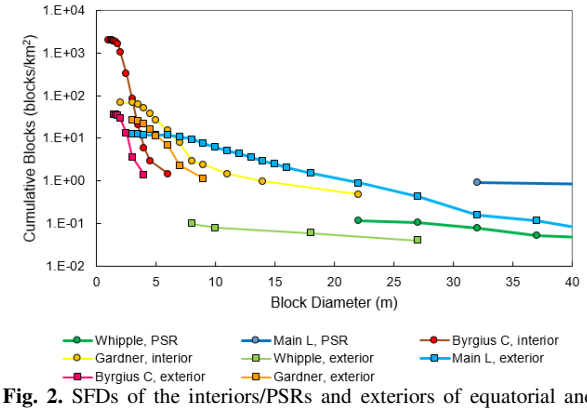


**Fig. 2.** SFDs of the interiors/PSRs and exteriors of equatorial and PSR-bearing lunar craters derived from this study.

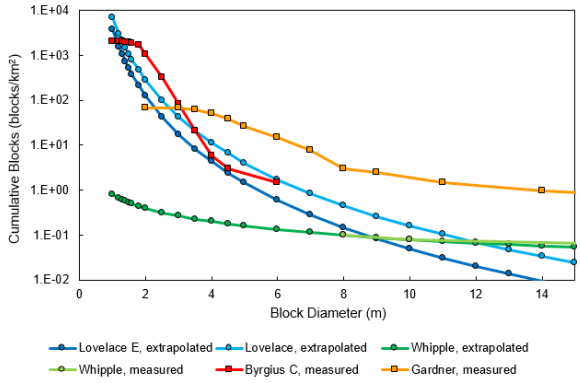


**Fig. 3.** Cumulative block distributions for small (<15 m) blocks. Pixel scale prevented direct counts of blocks <20 m, so a power law **[11]** was used to extrapolate their abundance.

**Discussion:** Double-bounce backscatter, a sign of ice, was not exclusively observed at PSR-bearing craters, preventing a definitive identification of craters containing significant water-ice deposits. Rozhdestvenskiy N had the highest double-bounce signature and no detectable blocks (20-m scale), and is therefore the most likely crater in this study to harbor ice deposits. However, a CPR enhancement in its interior (indicative of water ice) has not been observed **[12]**. Other craters contained double-bounce backscatter in patches, and these regions may be ice deposits, eroding slopes within PSRs, or hidden, sub-surface clasts. Low double-bounce backscatter does not necessarily preclude the presence of water ice. Ice diffused within the regolith could be present but undetectable by current remote sensing methods.

Because the interiors of young/fresh craters and older craters with ice could appear the same in radar, exterior block abundances were compared to estimate the likelihood of blocks in PSRs. All polar craters showed fewer blocks in their PSRs than exteriors; however, equatorial craters (Gardner and Byrgius C) showed the same trend, indicating that this is an inherent property of craters and not a result of ice, lighting conditions, or other latitude-dependent factors. Block counts show similar block sizes and densities between CPR-normal polar and CPR-anomalous equatorial craters. There is no statistically significant variation in *B* values between all types of craters, preventing that metric from being a distinguishing factor between crater types.

**Conclusions:** Most blocks observed in equatorial craters would be unresolvable in long-exposure NACs; therefore, blocks may still exist in craters classified here as block-free. SFDs did not reveal substantial differences between craters. The lack of consistent double-bounce backscatter in potential ice-bearing PSRs in this study indicates two possibilities: 1) not all lunar PSRs have water ice, or 2) there is water ice, but the physical state of the deposits is not detectable through this type of analysis. Future work should include *m-chi* maps and block counts of other polar CPR-anomalous craters to assess the presence of ice, including those at the south pole.

**References:** [1] Paige, D. A. et al. (2010a) *Sci., 330, 479-482.* [2] Sanin, A. et al. (2012) *JGR, 117.* [3] Lucey, P. et al. (2014) *JGR-P, 119, 1665-1679.* [4] Colaprete, A. et al. (2010) *Sci., 330, 463.* [5] Spudis, P. D., et al. (2013) *JGR-P, 118, 2016-2029.* [6] Raney, R. K. et al. (2011), *IEEE, 99, 808*-823. [7] Robinson, M. S. et al. (2010), *Sp. Sci. Rev., 150, 81-124.* [8] Koeber, S. D. et al. (2014) *LPS XLV*, Abst. # 2811. [9] Raney, R. K. et al. (2012) *JGR-P, 117.* [10] Kneissl, T. S. et al. (2011) *Plan. Sp. Sci., 59, 1243-1254.* [11] Hartmann, W. K. (1969) *Icarus*, *10, 201-213.* [12] Fa and Cai (2012) *JGR-P, 118, 1582–1608.*